NANO LETTERS

Letter

pubs.acs.org/NanoLett

High-Rate, Ultralong Cycle-Life Lithium/Sulfur Batteries Enabled by Nitrogen-Doped Graphene

Yongcai Qiu,[†] Wanfei Li,[†] Wen Zhao,[§] Guizhu Li,[†] Yuan Hou,[†] Meinan Liu,[†] Lisha Zhou,[†] Fangmin Ye,[†] Hongfei Li,[†] Zhanhua Wei,[‡] Shihe Yang,[‡] Wenhui Duan,[§] Yifan Ye,[∥] Jinghua Guo,[∥] and Yuegang Zhang*[,†,§]

[†]*i-LAB*, Suzhou Institute of Nano-Tech and Nano-Bionics, Chinese Academy of Sciences, Suzhou, Jiangsu 215123, China

[‡]Department of Chemistry, The Hong Kong University of Science and Technology, Kowloon, Hong Kong, China

[§]Department of Physics, Tsinghua University, Beijing 100084, China

[∥]The Advanced Light Source, Lawrence Berkeley National Laboratory, Berkeley, California 94720, United States

Supporting Information

ABSTRACT: Nitrogen-doped graphene (NG) is a promising conductive matrix material for fabricating high-performance Li/S batteries. Here we report a simple, low-cost, and scalable method to prepare an additive-free nanocomposite cathode in which sulfur nanoparticles are wrapped inside the NG sheets (S@NG). We show that the Li/S@NG can deliver high specific discharge capacities at high rates, that is, ~1167 mAh g^{-1} at 0.2 C, ~1058 mAh g^{-1} at 0.5 C, ~971 mAh g^{-1} at 1 C, ~802 mAh g^{-1} at 2 C, and ~606 mAh g^{-1} at 5 C. The cells also demonstrate an ultralong cycle life exceeding 2000 cycles and an extremely low capacity-decay rate (0.028% per cycle), which is among the best performance demonstrated so far for Li/S cells. Furthermore, the S@NG cathode can be cycled with an excellent Coulombic efficiency of above 97% after 2000 cycles. With a high active S content (60%) in the total electrode weight, the S@NG cathode could provide a specific energy that is competitive to the state-of-the-art Li-ion cells even after 2000 cycles. The X-ray spectroscopic analysis and ab initio calculation results indicate that the excellent performance can be attributed to the well-restored C−C lattice and the unique lithium polysulfide binding capability of the N functional groups in the NG sheets. The results indicate that the S@NG nanocomposite based Li/S cells have a great potential to replace the current Li-ion batteries.

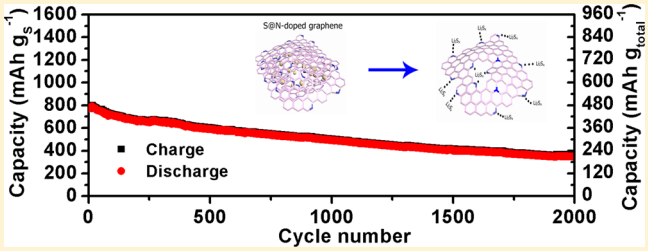

KEYWORDS: *Nitrogen-doped graphene, sulfur nanoparticles, specific capacity, cycle life, lithium/sulfur batteries*

Lithium/sulfur (Li/S) batteries have attracted considerable attention due to its great potential to deliver two to three times the energy density of current lithium-ion batteries.[1−3] Because the electrochemical redox reactions in a Li/S cell are based on a two electron reaction ($S + 2Li^+ + 2e^- \leftrightarrow Li_2S$), the corresponding theoretical specific capacity and energy density are as high as 1675 mA h g^{-1} and 2600 Wh kg^{-1}, respectively. However, the poor intrinsic electrical conductivity of the active material, the high solubility of intermediate polysulfides into the electrolyte, and the large volumetric expansion of approximately 76% based on full transformation of sulfur to Li_2S result in the low utilization of sulfur and the rapid capacity fading on cell cycling, which has hindered the further development of Li/S battery technology and its application.

To address these key issues, chemists and materials scientists have been trying to design and construct novel micro-structured/nanostructured S cathode materials to improve cell performance.[4−12] To improve the electrical conductivity of the S cathode and alleviate the dissolution of intermediate polysulfides, a variety of carbon structures such as carbon nanotubes, porous carbon, graphene, and carbon fibers have been developed as the matrix of S.[13−17] For example, Lou et al. and Nazar et al. have employed bimodal-carbon spheres to encapsulate nanostructured S, achieving a high and relatively stable discharge capacity of 850 mA h g^{-1} at a high current rate of 1 C after 100th cycling.[7,18] The advantage of the optimized bimodal-carbon spheres is that the smaller pores can entrap the sulfur while the larger pores facilitate electrolyte's access throughout the structure. More recently, the core/shell, yolk/shell, and other related structures have shown their benefit in accommodating the volumetric expansion of S during cycling.[12,19−24] For instance, Cui et al. have demonstrated that S@TiO_2 and S@PVP yolk/shell nanoarchitectures could improve the cycling stability of S cathode.[20,21] Despite of these progresses, achieving Li/S batteries with a high rate and a long cycling life is still difficult.

Graphene has emerged as one of the most promising conductive matrixes for Li/S batteries owing to its unique two-dimensional morphology, high specific surface area of over 2600 m^2/g, superior electrical conductivity, and excellent

Received: June 1, 2014
Revised: July 17, 2014
Published: July 29, 2014

ACS Publications © 2014 American Chemical Society

structural stability.[13,25−27] Recently, our group found that cetyltrimethylammonium bromide (CTAB) modified graphene oxide (GO)-S nanocomposite cathode could significantly improve the cycle life of the Li/S cells to 1,500 cycles.[28,29] However, low-temperature reduced GO in the previous work was not able to achieve high enough electrical conductivity, and it was necessary to add 10−20 wt % carbon black additives in the cathode to improve its conductivity that led to a lower S content percentage in the final cathode. We also find that it is necessary to develop a more simple and scalable approach to preparing highly conductive S/C composite materials for achieving high capacity over long-term cycling. Despite of the progress on the Li−ion battery research that used N-doped graphene−metal oxide nanocomposites,[30] there has been little success in using N-doped graphene-S nanocomposite to achieve Li/S cells with high capacity and long cycle life.[31,32] The achieved best performance for Li/NG-S cells was about 671 mA h g^{-1} after 200 cycles at a current rate of 1500 mA g^{-1} (~0.9 C).

In this report, we prepared a cathode comprising N-doped graphene wrapped S and PVDF binder only, without additional carbon black additives. First, we used a modified Hummers' method to synthesize GO sheets that consist of basal plane carbon atoms decorated with epoxy and hydroxyl groups and edge carbon atoms attached by carbonyl and carboxyl groups.[33,34] The tapping-mode atomic force microscope (AFM) image clearly shows that the as-prepared GO sheets are only one carbon layer thick (Supporting Information, Figure S1). Second, the freeze-dried GO sheets were subjected to a thermal nitridation process in NH_3 atmosphere at 750 °C for 30 min. After thermal nitridation, the oxygenated functional groups on the graphene oxide sheets were decomposed and partially transformed to N functional groups (Figure 1). The as-

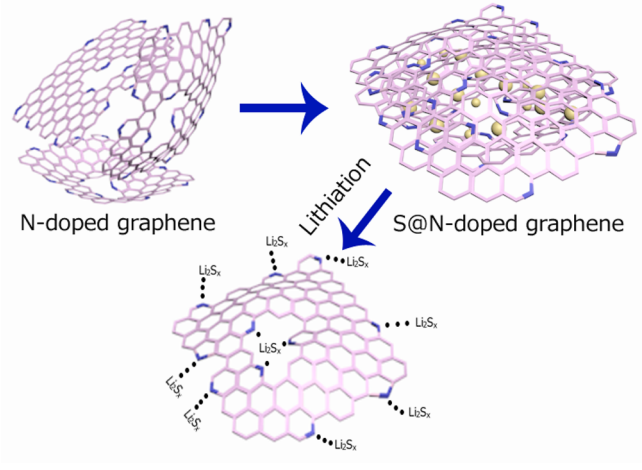

Figure 1. Proposed synthesis route for creating S@NG nanocomposite and N functional groups for trapping Li_2S_x.

obtained N-doped graphene (NG) is highly electrical conductive due to the restoration of the graphene network, which has been demonstrated by our previous reports.[25,27] The electrical conductivity of NG sheets is measured to be ~270 S cm^{-1} (Supporting Information, Table S1), which is much higher than those of the reduced GO sheets obtained by the hydrazine-reduction method or other thermal treatment methods.[35,36] Third, a facile and green chemical deposition method is used to wrap S into the NG sheets (S@NG). The reaction is described as $2Na_2S + Na_2S_2O_3 + 6HCOOH = 4S + 6HCOONa + 3H_2O$. To obtain ultrafine S particles, the reaction was carried out under 0 °C. Finally, the dried S@NG nanocomposite was mixed with PVDF binder to make cathodes for Li/S cells. The designed nanocomposite cathodes should have the following merits: (a) the highly conductive NG sheets with a large surface area are able to wrap S nanoparticles, resulting in significantly improved electronic conductivity of the overall S cathode even without using carbon black additives; (b) the self-generated curvature and wrinkles of the NG sheets inevitably bring out many cavities, which can facilitate electrolyte access throughout the structure and accommodate the volume change of S during charge/discharge; and (c) the strong ionic attraction between the N functional groups of NG sheets and the intermediate higher-order lithium polysulfides could help to trap these species, and/or affect their redeposition process upon discharge/charge (Figure 1).[37,38,50]

The scanning electron microscopy (SEM) images in Figure 2A and its inset show the porous structure of the S@NG

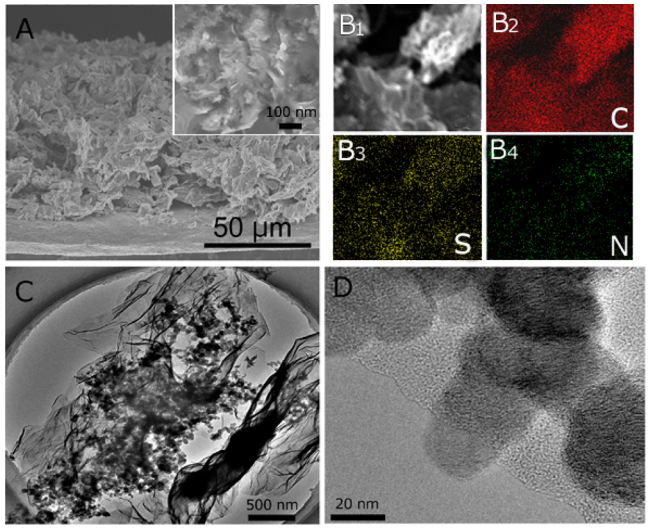

Figure 2. (A) Low- and high- (inset) manification SEM images of the S@NG nanocomposite. (B) EDX elemental mapping for C (B2), S (B3), and N (B4) from the same area shown in the dark field image (B1). (C) Low- and (D) High-magnification TEM images of the S@NG nanocomposite.

nanocomposite, where almost no apparent S particle can be observed on the curved and wrinkled surfaces of the NG sheets. On the other hands, the elemental mapping by energy-dispersive X-ray (EDX) analysis and the transmission electron microscopic (TEM) images show that S nanoparticles are uniformly distributed in the NG matrix (Figure 2B−D), indicating a large proportion of S is embedded in the NG sheets. The Brunauer−Emmett−Teller (BET) surface area of NG sheets is evaluated to be 643.5 m^2 g^{-1}, which is similar to our previous report.[30] The pore size distribution of the NG sheets is in the range of 3−30 nm with a sharp peak centered at 5 nm and a broad peak at around 10−30 nm, as estimated from the Barrett−Joyner−Halenda (BJH) equation (Supporting Information, Figure S2). The smaller pores are apt to trap intermediate polysulfides while the larger pores facilitate electrolyte ingress throughout the structure. To evaluate the S content in the S@NG nanocomposite, thermogravimetric analysis (TGA) was carried out under N_2 atmosphere with a heating rate of 10 °C min^{-1}. As shown in Supporting

dx.doi.org/10.1021/nl5020475 | Nano Lett. 2014, 14, 4821−4827

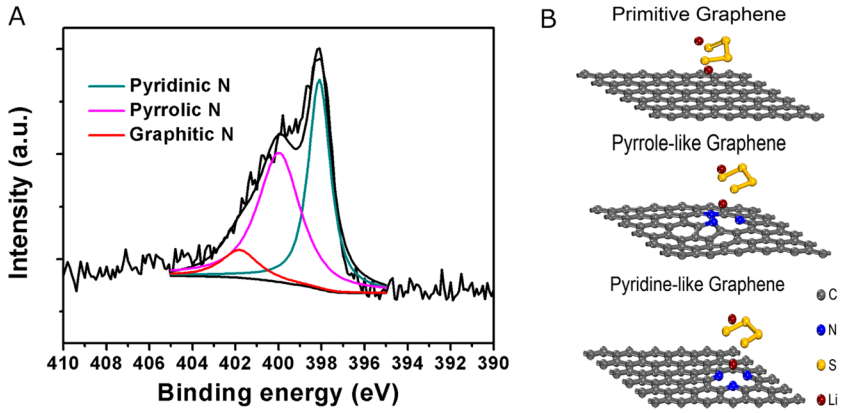

Figure 3. (A) High-resolution N 1s XPS spectrum of the NG sheets. (B) The ab initio calculated structures of Li_2S_4 adsorption on the primitive graphene, pyrrole-like graphene, and pyridine-like graphene, respectively.

Information, Figure S3, the TGA trace indicates that the S@NG nanocomposite has 65.2 wt % sulfur loading. The powder XRD pattern in Supporting Information, Figure S4 confirms that the as-deposited S belongs to the orthorhombic sulfur phase (JCPDS card no. 24-0733). The overlapped broad peak at about 26° can be attributed to the NG sheets from thermal restoration of sp^2 carbon. The high-magnification TEM image in Figure 2D shows that the low-temperature deposited S has a grain size of about 25 nm. This is distinct from our previous reports of the CTAB-modified GO-S nanocomposite, where the S was homogeneously distributed on the surfaces of GO and protected by CTAB surfactants.[28,29] The small grain size of S is believed to one of the key factors that enable the good performance of Li/S cells.[18]

The reconstituted N functional groups of NG sheets are vital for trapping intermediate higher-order lithium polysulfides or improving their redeposition process upon discharge/charge, through the strong $S_xLi^{\cdots}N$ interactions (Figure 1). The high-resolution N 1s XPS spectrum of the NG sheets can be deconvoluted into three different signals with binding energies of 399.1, 400.0, and 401.8 eV, corresponding to pyridinic N, pyrrolic N, and graphitic N, respectively (Figure 3).[39−41] The first two N types are dominant in the product, which are believed to be more effective in forming $S_xLi^{\cdots}N$ interactions via the N lone-pair electrons, resulting in alleviating dissolution of lithium polysulfides in the electrolyte and improving their redeposition process upon discharge/charge, thereby improving performance of the Li/S cells.[37,38] The role of N doping in immobilizing lithium polysulfides (Li_2S_x, x = 1, 4, 6, 8) was further confirmed by the ab initio calculations (see detailed computation method and Table 1 in the Supporting Information). The results show that NG sheets bind Li_2S_x much more strongly compared to the primitive graphene case (see Table 1). The enhancement is mostly due to the strong ionic attractions between N and Li cations, instead of that between N and S anions (Figure 3B and Table 1). The bonding energy between atomic Li and NG is much larger than that of the molecular Li and NG; and the bonding length of Li−S is only slightly increased from 2.4 to ∼2.6 Å after $S_xLi^{\cdots}N$ bond formation, indicating that the lithium polysulfide is trapped as a whole molecule.

Table 1. Comparisons of the Binding Energies for Primitive Graphene, Pyrrole-Like Graphene, and Pyridine-Like Graphene with Atomic Lithium and Lithium Polysulfides

E_{bind} (eV)	primitive graphene (A)	pyrrole-like graphene (B)	pyridine-like graphene (C)
Li	1.81	4.41	4.41
Li_2S	0.60	2.09	2.10
Li_2S_4	0.25	1.33	1.48
Li_2S_6	0.36	1.97	2.08
Li_2S_8	0.50	1.74	1.82

The oxidized N and/or other oxygenous species are almost absent in the N 1s XPS spectrum, suggesting excellent N doping of the NG sheets after thermal nitridation. Furthermore, a sharp C 1s XPS peak at ∼285.4 eV is detected (see Supporting Information, Figure S5), indicating a domination of sp^2-type C−C bonding in the NG sheets. The presence of O 1s can be attributed to the atmospheric O_2, CO_2, or moisture adsorbed on the NG sheets. The atomic ratio of nitrogen to carbon (N/C) in the NG sheets was estimated to be ∼3.9% from the peak areas of C 1s and N 1s. This N/C ratio is similar to that reported in the NG materials with good physiochemical activity and electrical conductivity.[42−44]

Utilizing the high electrical conductivity of NG sheets, the S@NG nanocomposite was directly mixed with 8% PVDF binder to produce electrodes without other carbon additives. The S content is ∼60% in the total electrode weight. It should be noted that the S content in the total cathode weight is a key parameter for a practical cell. A higher S content directly translates to a higher specific energy of a practical cell. The S@NG based cathodes, microporous polypropylene separators, and Li metal anodes were used to assemble the 2025-type coin cells in an Ar-filled glovebox. $LiNO_3$ was added to the electrolyte as additive as it has been proved to passivate the lithium anode surface and therefore reduce the shuttle effect.[45−47] An average sulfur loading in the electrode is approximately 0.8 mg cm^{-2}, similar to our previous reports.[28,29] The Li/S@NG cells were examined by cyclic voltammetry (CV) at a scan of 0.05 mV s^{-1} in the potential range of 1.5−2.8 V (vs Li/Li^+). As shown in Figure 4A, the first broad reduction peak at 2.26 V corresponds to the reduction of S_8 to higher-order Li polysulfides (Li_2S_x, $4 \le x \le 8$); The second reduction peak at 2.03 V is attributed to the further reduction of the higher-order Li polysulfides to insoluble Li_2S. A strong oxidation peak centered at 2.47 V corresponds to delithation processes from Li_2S to Li_2S_x and eventually to S_8. The reversible processes were found in the following cycles (Figure 4A). It is worth noting that the two reduction peaks in the

dx.doi.org/10.1021/nl5020475 | Nano Lett. 2014, 14, 4821−4827

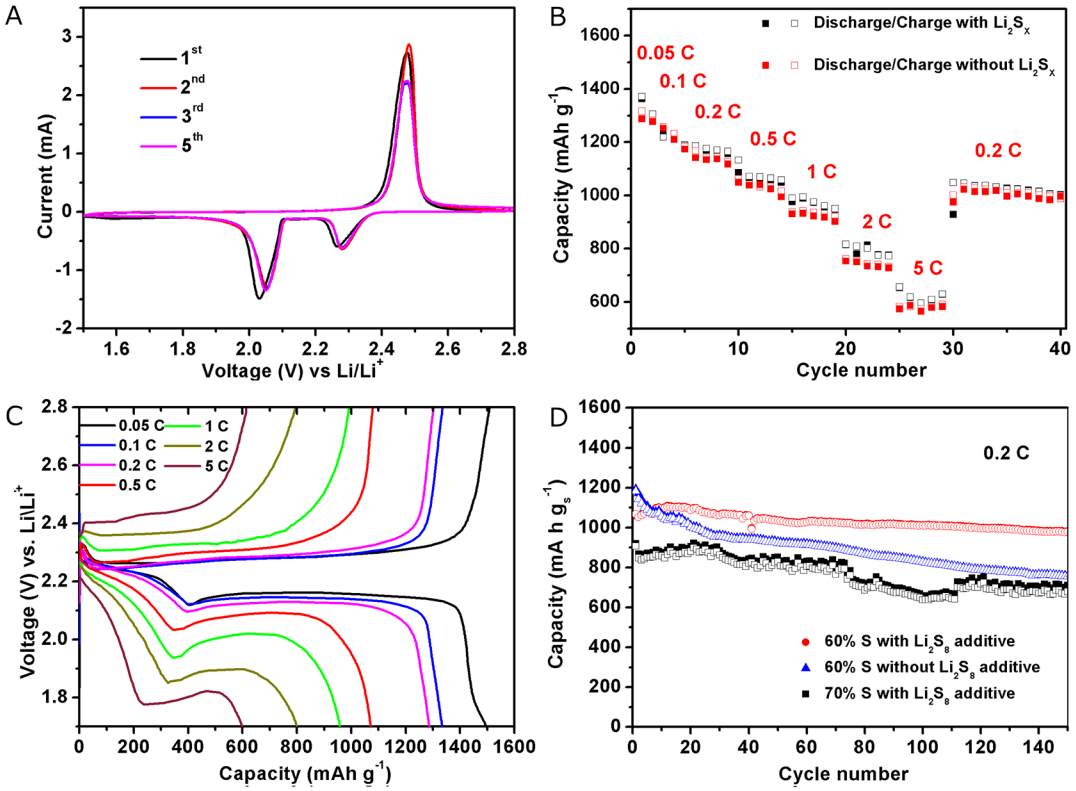

Figure 4. (A) CV profile of the S@NG electrode at a scan of 0.05 mV S^{-1}. (B) The rate performance comparisons between the S@NG electrode with and without Li_2S_8 additive and (C) its corresponding voltage-capacity profiles of the S@NG electrode with Li_2S_8 additive at various discharge/charge current rates. (D) Cycling performance comparisons between the 60% (S/total electrode weight) S@NG electrode with and without the Li_2S_8 additive, and 70% (S/total electrode weight) S@NG electrode with the Li_2S_8 additive cycled at 0.2 C.

subsequent cycles shift to higher potentials at 2.28 and 2.05 V, respectively, suggesting a reduced polarization after the first activation cycle.

Next, the Li/S@NG cells were evaluated by galvanostatic discharge/charge at various current rates. As shown in Figure 4B, the Li/S@NG cell with the Li_2S_8 additive in the electrolyte exhibited excellent rate performance. The Li_2S_8 additive in the electrolyte contributed ~0.128 mg of S to each Li/S cell, which was approximately 8.8 wt % sulfur in the cell. Assuming all S in the electrolyte contributed to the cell's capacity, we evaluated the specific capacity by the total S weight included both in the S@NG and in Li_2S_8 additive. To ensure a fair comparison of specific capacities, this evaluation method was used throughout this manuscript whenever Li_2S_8 additive was added in the electrolyte. The initial specific capacity of the cell was ~1366 mA h g_S^{-1} (by total S weight in the S@NG and the Li_2S_8 additive) at a rate of 0.05 C, nearly 81.5% of the theoretical capacity of S. The 1 C-rate is defined as the current density of 1675 mA g^{-1}. When the rate was changed to 0.1 C, a specific capacity of ~1231 mAh g^{-1} was retained, which was then slowly reduced to ~1167 mA h g^{-1} at 0.2 C, ~1058 mA h g^{-1} at 0.5 C, ~971 mA h g^{-1} at 1 C, ~802 mA h g^{-1} at 2 C, ~606 mA h g^{-1} at 5 C, and finally recovered to ~1030 mA h g^{-1} at a rate of 0.2 C. In contrast, the Li/S@NG cell without the Li_2S_8 additive showed slightly lower specific capacity at each rate stages, indicating a positive effect of the Li_2S_8 additive. It is believed that the role of Li_2S_8 additive is two-fold. One is that the lithium polysulfides in the electrolyte will help alleviating the dissolution of intermediate lithium polysulfides from the cathode during charge/discharge. The other is that they can provide reversible capacities during charge/discharge. Some studies show that Li/S cells work through a dissolution−precipitation mechanism to achieve reversible charge/discharge.[48,49] Therefore, extra soluble polysulfides would definitely facilitate the operation of Li/S cells.[50] Nevertheless, the rate capabilities of the Li/S@NG cells with and without Li_2S_8 additives are both at least on a par with the best performance reported for Li/S cells.[51,52]

Figure 4C shows its corresponding discharge/charge voltage profiles of the Li/S@NG cell at different current rates (0.05, 0.1, 0.2, 0.5, 1, 2, and 5 C) in the potential range of 1.7−2.8 V. The discharge profiles of all current densities were characterized by a two-plateau behavior of a typical S cathode, which is in good agreement with CV curves.[4,53] It can be noticed that both the discharge voltage plateau and the discharge capacity decrease gradually with increasing current rate, which can be ascribed to higher ohmic and kinetic overvoltage at higher current rate. The high S utilization and the excellent rate performance are likely due to the wrapping of ultrafine S nanoparticles by the highly conductive NG sheets. To further understand the effect of Li_2S_8 additive in the electrolyte, the S@NG electrode (60% S content by total electrode weight) with and without the Li_2S_8 additive was cycled at a current rate of 0.2 C. As shown in Figure 4D, the S@NG electrode with the Li_2S_8 additive remained a discharge capacity of above 978 mAh g_s^{-1} after 150 cycles, representing a capacity loss of 11.1%, while without Li_2S_8 additive, the S@NG electrode decreased to about 760 mAh g_s^{-1} after 150 cycles, corresponding to a capacity loss of 35.6%. Even for the S@NG electrode with 70% S content, it could still deliver a capacity of above 680 mAh g_s^{-1} after 150

dx.doi.org/10.1021/nl5020475 | Nano Lett. 2014, 14, 4821−4827

cycles, corresponding to a capacity loss of 24.5%. The results, again, indicate a positive effect of the Li_2S_8 additive on the performance of Li/S cells.

Good capacity retention over long cycles is crucial for the practical implementation of Li/S batteries. Figures 5 and 6

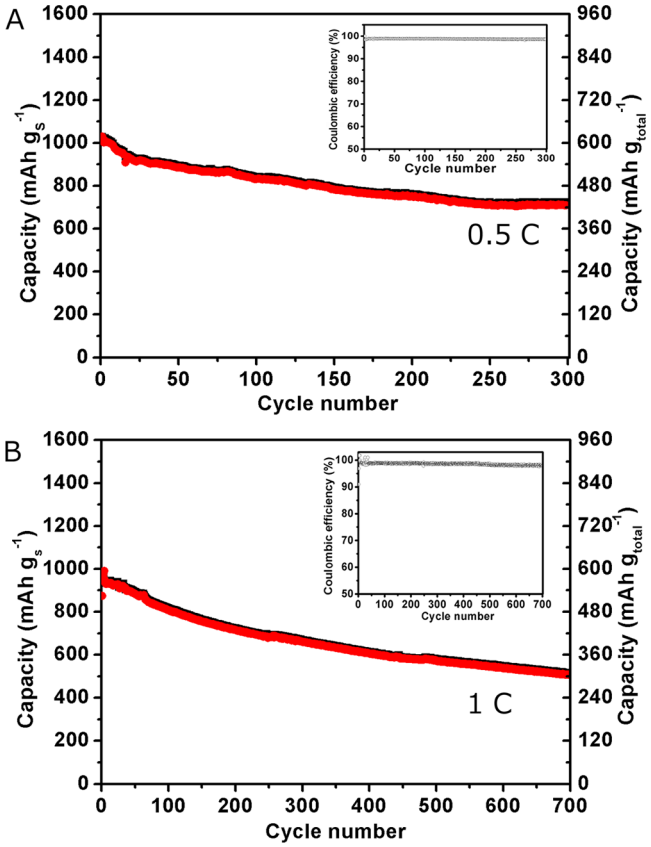

Figure 5. Cycling performance tests of the S@NG electrode at 0.5 C (A) and 1 C (B) current rates, respectively. Insets of panels A and B are their corresponding Coulombic efficiencies at 0.5 and 1 C current rates, respectively.

show the cycling performance of the Li/S@NG cells. At a current rate of 0.5 C, an initial specific capacity of ~1030 mAh g_s^{-1} (by total S weight in the S@NG and the Li_2S_8 additive) was achieved. This capacity decreased to about 830 mAh g_s^{-1} after 100 cycles, representing a capacity loss of 19.5%, and to about 752 mAh g_s^{-1} after 200 cycles, indicative of a 27.0% capacity loss. Even after 300 cycles, the capacity remained above 752 mAh g_s^{-1}, corresponding to a capacity retention of 69.3%. In the case that the total electrode mass (including inactive materials, such as NG and binder) is considered, the specific capacity of our cathode is ~429 mAh g_{total}^{-1} (M_{total} = M_{Sulfur} + M_{NG} + M_{binder}) after 300 cycles, which is still higher than that of the best cathode in current Li-ion cells. Additionally, the Li/S@NG cell also maintained a high Coulombic efficiency even after 300 cycles, and the average over 300 cycles was about 98.3% at 0.5 C (inset of Figure 5A). When the current rate was increased to 1 C, an initial capacity of about 874 mAh g_s^{-1} was achieved. After four cycles of activation, the cell reached its highest capacity of about 967 mAh g_s^{-1} (580 mAh g_{total}^{-1}). A discharge capacity of about 808 and 573 mAh g_s^{-1} can be obtained after 100 and 500 cycles, corresponding to capacity retention of 83.6 and 59.3% of its highest capacity, respectively. After 700 cycles, the cell still delivered a reversible discharge capacity of 506 mAh g_s^{-1} (304 mAh g_{total}^{-1}), corresponding to capacity retention of 52.4%. The capacity decay was as low as 0.068% per cycle. The average Coulombic efficiency of the cell at 1 C was still above 98.0% (inset of Figure 5B).

To further demonstrate the remarkable cycling stability of the S@NG electrode, we cycled a Li/S@NG cell up to 2000 cycles under a higher current rate of 2 C (Figure 6A). The cell reached its highest specific capacity of about 789 mAh g^{-1} (473 mAh g_{total}^{-1}) at the 15th cycle, and the discharge capacity stabilized at 730 mAh g_s^{-1} after 50 more cycles. The capacity decreased to 711 mAh g_s^{-1} after 100 cycles, corresponding to a capacity loss of only 9.9%, and to 589 mAh g_s^{-1} after 500 cycles, corresponding to a capacity loss of 25.3%. The capacity decay was as low as 0.051% per cycle in the first 500 cycles. After 1000 cycles, the discharge capacity still remained about 492 mAh g^{-1}, corresponding to a capacity fade of 37.7% and only 0.038% loss per cycle. A discharge capacity of about 406 and 347 mAh g_s^{-1} can be obtained after 1500 and 2000 cycles, corresponding to capacity retention of 51.4 and 44.0% of its highest capacity, respectively. The overall capacity decay was as low as 0.028% per cycle. In addition, the Coulombic efficiency of the cell still remained 97.1% after 2000 cycles (inset of Figure 6A). These results suggest that the shuttling effect could be more effectively restrained at a higher current rate because of a faster discharge/charge process. It should be mentioned that the discharge voltage plateau gradually recover from 1.89 to 2.03 V (Figure 6B), suggesting a slow activation of the S@NG nanocomposite with increasing cycle times, probably because of S redistribution on NG sheets during discharge/charge (see the previous discussion on the role of N-doping). Another synergic effect of the porous NG sheets is to accommodate the volumetric expansion of S upon discharge/charge. As shown in the cross-sectional SEM images (Supporting Information, Figure S6), the pristine S@NG cathode has an initial thickness of ~30 μm. After 100 charge/discharge cycles and at the fully discharged state, the electrode thickness is almost unchanged, indicative of no volume expansion induced structure destruction at the electrode level. These results demonstrate that the synergic effect of the N-doping, high surface area, and high conductivity of the NG sheets could play a role of "self-healing" for the electrode, which makes NG a promising matrix material for fabricating high performance Li/S batteries.

To further confirm the role of the N functional groups, we prepared a control sample using thermally reduced graphene sheets. The graphene sheets (GS) without nitrogen doping were prepared by directly thermal treatment of GO in Ar atmosphere at 750 °C. The S@GS nanocomposite as the control sample was prepared using the same S deposition method as the S@NG preparation, and a Li/S@GS cell was assembled in the same way as described above. As shown in Supporting Information, Figure S7, the Li/S@GS cell only delivered an initial capacity of about 870 mAh g_S^{-1} at 0.5 C, and 734 mAh g_S^{-1} after 100 cycles. The value is much lower than the Li/S@NG cell. The Coulombic efficiency of the S@GS cell is also much lower (~94.9%). The comparison indicates that GS without N functional groups is not as effective as NG in preventing lithium polysulfide shuttling.

The role of N functional groups in lithium sulfide immobilization was also supported by the X-ray absorption spectroscopy (XAS) measurement results. Supporting Information, Figure S8 displays the S K-edge and N K-edge total

dx.doi.org/10.1021/nl5020475 | Nano Lett. 2014, 14, 4821−4827

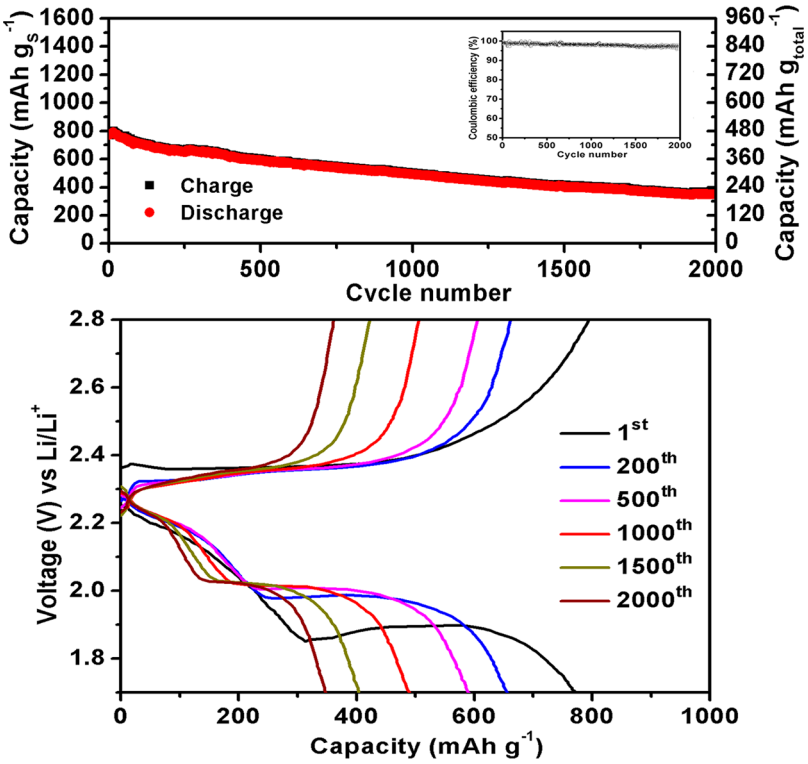

Figure 6. (A) Long-term cycling performance test of the S@NG electrode at 2 C discharge/charge rate. Inset is its corresponding Coulombic efficiency at 2 C. (B) The corresponding voltage-capacity profiles at different cycles.

fluorescence yield-near edge X-ray absorption fine structure spectra of the S@NG cathode materials before and after 200 charge/discharge cycles. The S K-edge spectral feature at 2472.0 eV in the pristine sample (Supporting Information, Figure S7A) can be deconvoluted into two peaks centered at 2471.9 and 2473.4 eV, respectively. The former can be attributed to the transition from the S 1s core level to the S−S π^* states of elemental S, and the latter corresponds to the transition from the S 1s to the C−S σ^* states.[54,55] The N K-edge spectrum in the pristine sample (Supporting Information, Figure S7B) further confirms the existence of three types of N doping, which is consistent with the XPS analysis mentioned above. The first two features centered at 397.1 and 399.9 eV arise from transitions from the K shell (N 1s) to unoccupied π^* orbital containing N character (pyridinic N, pyrrolic N, and graphitic N) and the peak at 406.1 eV corresponds to the transition into σ^* orbital.[56] However, at the fully discharged state after 200 cycles, the C−S bond feature disappears in the S K-edge spectrum, and a new peak at 398.5 eV emerges in the N K-edge spectrum, which is quite different from our previous observation for GO-S nanocomposite.[28,55] This could be explained by the lithiation of S to Li_2S_2 or Li_2S and the formation of N···Li_2S_x interactions as suggested by our ab initio calculation.

In conclusion, we designed and synthesized a S@NG nanocomposite material in which ultrafine S nanoparticles were wrapped in the highly conductive NG sheets. No additional carbon additive is needed to use this nanocomposite as a cathode for Li/S@NG cells. The cathode with 60% of S in the total electrode weight exhibited high specific capacity and excellent rate performance up to 5 C. We further demonstrated an ultralong cycle life up to 2000 cycles at 2 C with a decay rate of as low as 0.028% per cycle, which is one of the best performances reported so far to the best of our knowledge. The excellent performance is attributed to a variety of synergic effects, including the high surface area and high conductivity of the porous NG matrix, as well as the unique Li_2S_x binding capability of the N functional groups in the NG sheets. This work demonstrated that the S@NG electrode has a great potential to be used in low-cost and high-energy Li/S batteries.

■ ASSOCIATED CONTENT

Supporting Information

Full description of the material and other characterizations. This material is available free of charge via the Internet at http://pubs.acs.org.

■ AUTHOR INFORMATION

Corresponding Author

*E-mail: ygzhang2012@sinano.ac.cn.

Notes

The authors declare no competing financial interest.

■ ACKNOWLEDGMENTS

This work was supported by China Postdoctoral Science Foundation (No. 2014M550314) and the Natural Science Foundation of Jiangsu Province, China (No. BK20140383).

■ REFERENCES

(1) Kim, J.; Lee, D. J.; Jung, H. G.; Sun, Y. K.; Hassoun, J.; Scrosati, B. *Adv. Funct Mater.* **2013**, *23*, 1076−1080.

(2) Manthiram, A.; Fu, Y. Z.; Su, Y. S. *Acc. Chem. Res.* **2013**, *46*, 1125−1134.

(3) Song, M. K.; Cairns, E. J.; Zhang, Y. G. *Nanoscale* **2013**, *5*, 2186−2204.

(4) Li, G. C.; Li, G. R.; Ye, S. H.; Gao, X. P. *Adv. Energy Mater.* **2012**, *2*, 1238−1245.

(5) Ji, X. L.; Lee, K. T.; Nazar, L. F. *Nat. Mater.* **2009**, *8*, 500−506.
(6) Jayaprakash, N.; Shen, J.; Moganty, S. S.; Corona, A.; Archer, L. A. *Angew. Chem., Int. Ed.* **2011**, *50*, 5904−5908.
(7) Schuster, J.; He, G.; Mandlmeier, B.; Yim, T.; Lee, K. T.; Bein, T.; Nazar, L. F. *Angew. Chem., Int. Ed.* **2012**, *51*, 3591−3595.
(8) Bresser, D.; Passerini, S.; Scrosati, B. *Chem. Commun.* **2013**, *49*, 10545−10562.
(9) Evers, S.; Nazar, L. F. *Acc. Chem. Res.* **2013**, *46*, 1135−1143.
(10) Zu, C. X.; Manthiram, A. *Adv. Energy Mater.* **2013**, *3*, 1008−1012.
(11) Zhao, C. Y.; Liu, L. J.; Zhao, H. L.; Krall, A.; Wen, Z. H.; Chen, J. H.; Hurley, P.; Jiang, J. W.; Li, Y. *Nanoscale* **2014**, *6*, 882−888.
(12) Wang, M. J.; Wang, W. K.; Wang, A. B.; Yuan, K. G.; Miao, L. X.; Zhang, X. L.; Huang, Y. Q.; Yu, Z. B.; Qiu, J. Y. *Chem. Commun.* **2013**, *49*, 10263−10265.
(13) Chen, R. J.; Zhao, T.; Lu, J.; Wu, F.; Li, L.; Chen, J. Z.; Tan, G. Q.; Ye, Y. S.; Amine, K. *Nano Lett.* **2013**, *13*, 4642−4649.
(14) Hwang, T. H.; Jung, D. S.; Kim, J. S.; Kim, B. G.; Choi, J. W. *Nano Lett.* **2013**, *13*, 4532−4538.
(15) Lu, S. T.; Cheng, Y. W.; Wu, X. H.; Liu, J. *Nano Lett.* **2013**, *13*, 2485−2489.
(16) Rong, J. P.; Ge, M. Y.; Fang, X.; Zhou, C. W. *Nano Lett.* **2014**, *14*, 473−479.
(17) Wang, L.; Dong, Z. H.; Wang, D.; Zhang, F. X.; Jin, J. *Nano Lett.* **2013**, *13*, 6244−6250.
(18) Zhang, C. F.; Wu, H. B.; Yuan, C. Z.; Guo, Z. P.; Lou, X. W. *Angew. Chem., Int. Ed.* **2012**, *51*, 9592−9595.
(19) Wang, J. Z.; Lu, L.; Shi, D. Q.; Tandiono, R.; Wang, Z. X.; Konstantinov, K.; Liu, H. K. *ChemPlusChem.* **2013**, *78*, 318−324.
(20) Seh, Z. W.; Li, W. Y.; Cha, J. J.; Zheng, G. Y.; Yang, Y.; McDowell, M. T.; Hsu, P. C.; Cui, Y. *Nat. Commun.* **2013**, *4*, 1331−1337.
(21) Li, W. Y.; Zheng, G. Y.; Yang, Y.; Seh, Z. W.; Liu, N.; Cui, Y. *Proc. Natl. Acad. Sci. U.S.A.* **2013**, *110*, 7148−7153.
(22) Zhang, Y. G.; Zhao, Y.; Konarov, A.; Gosselink, D.; Li, Z.; Ghaznavi, M.; Chen, P. *J. Nanopart. Res.* **2013**, *15*, 1−7.
(23) Miao, L. X.; Wang, W. K.; Wang, A. B.; Yuan, K. G.; Yang, Y. S. *J. Mater. Chem. A* **2013**, *1*, 11659−11664.
(24) Cai, K. P.; Song, M. K.; Cairns, E. J.; Zhang, Y. G. *Nano Lett.* **2012**, *12*, 6474−6479.
(25) Qiu, Y. C.; Yan, K. Y.; Yang, S. H.; Jin, L. M.; Deng, H.; Li, W. S. *ACS Nano* **2010**, *4*, 6515−6526.
(26) Sun, H.; Xu, G. L.; Xu, Y. F.; Sun, S. G.; Zhang, X. F.; Qiu, Y. C.; Yang, S. H. *Nano Res.* **2012**, *5*, 726−738.
(27) Qiu, Y. C.; Zhang, X. F.; Yang, S. H. *Phys. Chem. Chem. Phys.* **2011**, *13*, 12554−12558.
(28) Ji, L. W.; Rao, M. M.; Zheng, H. M.; Zhang, L.; Li, Y. C.; Duan, W. H.; Guo, J. H.; Cairns, E. J.; Zhang, Y. G. *J. Am. Chem. Soc.* **2011**, *133*, 18522−18525.
(29) Song, M. K.; Zhang, Y. G.; Cairns, E. J. *Nano Lett.* **2013**, *13*, 5891−5899.
(30) Wu, Z. S.; Zhou, G. M.; Yin, L. C.; Ren, W.; Li, F.; Cheng, H. M. *Nano Energy* **2012**, *1*, 107−131.
(31) Wang, C.; Su, K.; Wan, W.; Guo, H.; Zhou, H. H.; Chen, J. T.; Zhang, X. X.; Huang, Y. H. *J. Mater. Chem. A* **2014**, *2*, 5018−5023.
(32) Wang, X. W.; Zhang, Z.; Qu, Y. H.; Lai, Y. Q.; Li, J. *J. Power Sources* **2014**, *256*, 361−368.
(33) Hummers, W. S.; Offeman, R. E. *J. Am. Chem. Soc.* **1958**, *80*, 1339−1339.
(34) Xu, Y. X.; Bai, H.; Lu, G. W.; Li, C.; Shi, G. Q. *J. Am. Chem. Soc.* **2008**, *130*, 5856−5857.
(35) Wang, S. J.; Geng, Y.; Zheng, Q. B.; Kim, J. K. *Carbon* **2010**, *48*, 1815−1823.
(36) Pei, S. F.; Zhao, J. P.; Du, J. H.; Ren, W. C.; Cheng, H. M. *Carbon* **2010**, *48*, 4466−4474.
(37) Guo, J. C.; Yang, Z. C.; Yu, Y. C.; Abruna, H. D.; Archer, L. A. *J. Am. Chem. Soc.* **2013**, *135*, 763−767.
(38) Seh, Z. W.; Wang, H. T.; Hsu, P. C.; Zhang, Q. F.; Li, W. Y.; Zheng, G. Y.; Yao, H. B.; Cui, Y. *Energy Environ. Sci.* **2014**, *7*, 672−676.
(39) Shin, W. H.; Jung, H. M.; Choi, Y. J.; Miyasaka, K.; Kang, J. K. *J. Mater. Chem.* **2010**, *20*, 6544−6549.
(40) Zhang, L. S.; Liang, X. Q.; Song, W. G.; Wu, Z. Y. *Phys. Chem. Chem. Phys.* **2010**, *12*, 12055−12059.
(41) Sim, U.; Yang, T. Y.; Moon, J.; An, J.; Hwang, J.; Seo, J. H.; Lee, J.; Kim, K. Y.; Lee, J.; Han, S.; Hong, B. H.; Nam, K. T. *Energy Environ. Sci.* **2013**, *6*, 3658−3664.
(42) Wei, D. C.; Liu, Y. Q.; Wang, Y.; Zhang, H. L.; Huang, L. P.; Yu, G. *Nano Lett.* **2009**, *9*, 1752−1758.
(43) Lu, Y. F.; Lo, S. T.; Lin, J. C.; Zhang, W. J.; Lu, J. Y.; Liu, F. H.; Tseng, C. M.; Lee, Y. H.; Liang, C. T.; Li, L. J. *ACS Nano* **2013**, *7*, 6522−6532.
(44) Usachov, D.; Vilkov, O.; Gruneis, A.; Haberer, D.; Fedorov, A.; Adamchuk, V. K.; Preobrajenski, A. B.; Dudin, P.; Barinov, A.; Oehzelt, M.; Laubschat, C.; Vyalikh, D. V. *Nano Lett.* **2011**, *11*, 5401−5407.
(45) Xiong, S. Z.; Xie, K.; Hong, X. B. *Chem. J. Chin. Univ.* **2011**, *32*, 2645−2649.
(46) Xiong, S. Z.; Xie, K.; Diao, Y.; Hong, X. B. *Electrochim. Acta* **2012**, *83*, 78−86.
(47) Zhang, S. S. *J. Electrochem. Soc.* **2012**, *159*, A920−A923.
(48) Mikhaylik, Y. V.; Akridge, J. R. *J. Electrochem. Soc.* **2004**, *151*, A1969−A1976.
(49) Nelson, J.; Misra, S.; Yang, Y.; Jackson, A.; Liu, Y. J.; Wang, H. L.; Dai, H. J.; Andrews, J. C.; Cui, Y.; Toney, M. F. *J. Am. Chem. Soc.* **2012**, *134*, 6337−6343.
(50) Yao, H. B.; Zheng, G.; Hsu, P.; Kong, D.; Cha, J.; Li, W.; Seh, Z.; McDowell, M. T.; Yan, K.; Liang, Z.; Narasimhan, V.; Cui, Y. *Nat. Commun.* **2014**, *5*, 3943−3951.
(51) Barghamadi, M.; Kapoor, A.; Wen, C. *J. Electrochem. Soc.* **2013**, *160*, A1256−A1263.
(52) Yang, Y.; Zheng, G. Y.; Cui, Y. *Chem. Soc. Rev.* **2013**, *42*, 3018−3032.
(53) Wang, H. L.; Yang, Y.; Liang, Y. Y.; Robinson, J. T.; Li, Y. G.; Jackson, A.; Cui, Y.; Dai, H. J. *Nano Lett.* **2011**, *11*, 2644−2647.
(54) Ota, H.; Akai, T.; Namita, H.; Yamaguchi, S.; Nomura, M. *J. Power Sources* **2003**, *119*, 567−571.
(55) Zhang, L.; Ji, L. W.; Glans, P. A.; Zhang, Y. G.; Zhu, J. F.; Guo, J. H. *Phys. Chem. Chem. Phys.* **2012**, *14*, 13670−13675.
(56) McCann, R.; Roy, S. S.; Papakonstantinou, P.; Ahmad, I.; Maguire, P.; McLaughlin, J. A.; Petaccia, L.; Lizzit, S.; Goldoni, A. *Diamond Relat. Mater.* **2005**, *14*, 1057−1061.